Journal of ELECTRONIC MATERIALS, Vol. 47, No. 1, 2018
DOI: 10.1007/s11664-017-5859-0
© 2017 The Minerals, Metals & Materials Society

$(K_{0.5}Na_{0.5})NbO_3$-$Bi(Cu_{2/3}Nb_{1/3})O_3$ Lead-free Ceramics: Phase Transition, Enhanced Dielectric and Piezoelectric Properties

XIULI CHEN,[1,2] XIAO YAN,[1] GAOFENG LIU,[1] XIAOXIA LI,[1] GUISHENG HUANG,[1] and HUANFU ZHOU[1]

1.—Collaborative Innovation Center for Exploration of Hidden Nonferrous Metal Deposits and Development of New Materials in Guangxi, Guangxi Ministry-Province Jointly-Constructed Cultivation Base for State Key Laboratory of Processing for Non-ferrous Metal and Featured Materials, Guangxi Key Laboratory in Universities of Clean Metallurgy and Comprehensive Utilization for Non-ferrous Metals Resources, School of Materials Science and Engineering, Guilin University of Technology, Guilin 541004, China. 2.—e-mail: cxlnwpu@163.com

$(1-x)(K_{0.5}Na_{0.5})NbO_3$-$xBi(Cu_{2/3}Nb_{1/3})O_3$ [$(1-x)$KNN-xBCN, $0 \le x \le 0.02$] lead-free piezoelectric ceramics were prepared by a solid-state reaction method. The effects of BCN addition on the phase transition, microstructure and electrical properties of ceramics were studied. X-ray diffraction and Raman spectroscopy analysis confirmed that the BCN has diffused into KNN to form a solid solution. Both polymorphic phase transition, $T_{O\text{-}T}$, and Curie temperature, T_c, gradually decreased with increasing the BCN content. Moreover, the relative permittivity (ε_r) was increased greatly and the dielectric loss ($\tan\delta$) was almost decreased. Ferroelectric hysteresis loops (P–E) of samples showed that the remnant polarization (P_r) was up to a maximum value with 26.52 μm/cm as $x = 0.01$. The piezoelectric properties of ceramics increased with increasing the x values. When $x = 0.005$ and 0.01, the ceramics exhibited high piezoelectric constant with 131 pC/N and 105 pC/N over a good piezoelectric stability under 350°C, respectively. These results indicate that BCN addition is an effective way to enhance the properties of KNN ceramics.

Key words: $(K_{0.5}Na_{0.5})NbO_3$, dielectric properties, piezoelectricity, ferroelectric properties

INTRODUCTION

Piezoceramics are widely applied in modern electronic devices, such as high-performance actuators and transducers. $Pb(Zr_{1-x}Ti_x)O_3$ (PZT)-based ceramics have been the mainstay in the electronic device field because of their good dielectric performances, piezoelectric properties and electromechanical coupling coefficients. However, Pb can cause irreversible damage, even death, to the humans, so it is very urgent to search for environmentally friendly lead-free piezoceramics.[1–7]

Due to a high Curie temperature, T_C, and excellent dielectric performance, KNN lead-free ceramics could be a candidate to replace PZT. However, the dielectric thermal stability of pure KNN is poor and the piezoelectric properties are relatively low, restricting its further application.[8–11] In order to solve these issues, researchers often include some additives to change the internal phase structure of KNN, which could shift the $T_{O\text{-}T}$ to lower temperatures to optimize the thermal stability dielectric performance, creating materials to be used in high-temperature capacitors. Wang et al. reported that there are two approaches to improve the piezoelectric properties, by shifting the polymorphic phase transition (PPT) temperature, $T_{O\text{-}T}$, to well below room temperature, and by fabricating textured samples.[12,13] Although the morphotropic phase boundary (MPB) of PZT means the ceramics have remarkable thermal stability, it is not applicable for KNN-based lead-free ceramics due to the increased

(Received June 5, 2017; accepted October 3, 2017; published online October 23, 2017)

polarization anisotropy and to the energy barrier for polarization rotation deviating from MPB.[13] Therefore, shifting $T_{O\text{-}T}$ is a realizable method to optimize the piezoelectric properties of materials.

Adding additives to KNN would change the internal phase structure which works for the T_C and $T_{O\text{-}T}$ in ceramics, so that we can gobtain piezoelectric ceramics with excellent performance.[14–16] In this paper, BCN was added to KNN to enhance the properties of the materials. Furthermore, the effects of BCN addition on the phase, dielectric, ferroelectric and piezoelectric properties were also studied.

EXPERIMENTAL

$(1 - x)$KNN-xBCN $(0 \le x \le 0.02)$ ceramics were prepared by the solid-state sintering method as described in our previous work.[2] The KNN and BCN powders were calcined at 900°C for 8 h and 750°C for 4 h, respectively, and the sintering temperature ranging from 1130°C to 1160°C for 2 h in air. The electric field-induced polarization (P–E) and current (S–E) were measured by a ferroelectric test system (P-PMF; Radiant). Other test instrument models were as described in our previous work.[17]

RESULTS AND DISCUSSION

Figure 1a shows the X-ray diffraction (XRD) patterns of $(1 - x)$KNN-xBCN ceramics sintered at their optimized temperatures with a 2θ range of 20°–70°. It can be seen that the main peak is the pure perovskite structure of KNN, which indicates that the BCN has diffused into the KNN to form a homogeneous solid solution. The enlarged XRD patterns of $(1 - x)$KNN-xBCN ceramics in the range of 2θ from 44°–47° are demonstrated in Fig. 1b. The split of (202) and (020) peaks changed into (200), indicating that the phase structure changed from the orthorhombic to a pseudo-cubic system. When $x = 0.01$, the orthorhombic phase coexists with tetragonal phases, which reveals that there exists a MBP in this component, and thus the piezoelectric properties would be optimized. With increasing the x values to 0.02, the phase structure changed into a pseudo-cubic phase. The phase transition shows that the BCN has diffused into the KNN and formed a new internal phase.

Figure 2 illustrates the SEM pictures of $(1 - x)$KNN-xBCN $(0.005 \le x \le 0.015)$ ceramics sintered at their optimized temperatures. All samples are dense and few pores exist in the ceramics. BCN may act as the sintering aid by forming a liquid phase,[12,13] and thus the grains grow well. When $x = 0.01$, the ceramics exhibited the optimized microstructure and the grain size is 1–2 μm. However, the grain size decreased with further increasing the BCN content. When $x = 0.02$, the sintering behavior of the ceramics degraded greatly because the total binding force of dispersed phase particles is greater than the driving force of the grain boundary.

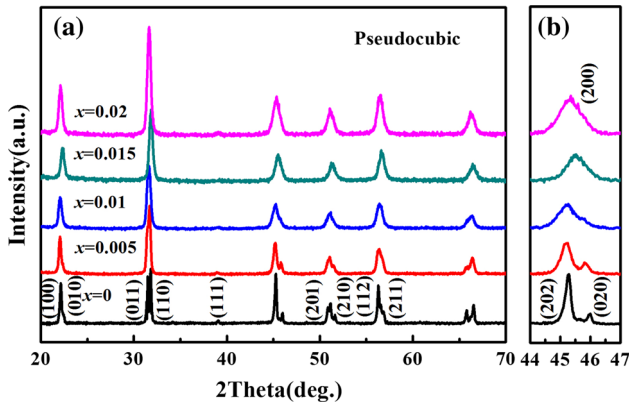

Fig. 1. (a) X-ray diffraction patterns of $(1 - x)$KNN-xBCN ceramics with $0 \le x \le 0.02$ at room temperature. (b) The enlarged XRD of $(1 - x)$KNN-xBCN ceramics in the range of 2θ from 44° to 47°.

Raman spectroscopy is very sensitive to the change of the solid phase structure, which can identify the transformation of the corresponding valence bond by detecting the characteristic peak of KNN-based materials.[18–20] In order to further identify the structure of $(1 - x)$KNN-xBCN ceramics, the Raman spectroscopy was measured and the results are demonstrated in Fig. 3. ν_1 (613 cm^{-1}), ν_5 (254 cm^{-1}), and $\nu_1 + \nu_5$ (860 cm^{-1}) appeared in the range of 200–900 cm^{-1}. In these regions, there is a strong pillow shoulder peak in the vicinity of the 613 cm^{-1} peak, which is the characteristic peak of the orthorhombic and tetragonal phases for KNN ceramics. The slope of the shoulder increased with increasing x values. Due to the changes in the vibrations of the NbO_6 octahedron in the crystal structure, the peak of the NbO_6 octahedron widened with increasing x values.[21–24]

Figure 4 shows the temperature dependences of the ε_r and tanδ for $(1 - x)$KNN-xBCN $(0 \le x \le 0.02)$ ceramics taken at 10 kHz from room temperature to 500°C. The $(1 - x)$KNN-xBCN $(x < 0.02)$ ceramics exhibited the orthorhombic–tetragonal ($T_{O\text{-}T}$) polymorphic phase transition and the tetragonal–cubic ferroelectric phase transition (T_c),[23–27] which were similar to the pure KNN ceramics. $T_{O\text{-}T}$ shifted to a lower temperature, which could expand the dielectric and piezoelectric temperature-stable intervals. The T_c shifted to a lower temperature from 400°C ($x = 0.005$) to 383°C ($x = 0.015$). When $x = 0.02$, T_c disappeared. In addition, the ε_r and tanδ of the $(1 - x)$KNN-xBCN ceramics were improved. When $x = 0.01$, the ceramics exhibited a maximum value of $\varepsilon \sim 6771$.

Figure 5 demonstrates the thermal stability of ε_r ($\Delta\varepsilon/\varepsilon_{120°C}$) for KNN–BCN sample ceramics. The addition of BCN could optimize the $\Delta\varepsilon/\varepsilon_{120°C}$ of the ceramics. Especially, when $x = 0.01$, the samples have a high ε_r ($\sim$ 1502), low tanδ ($\le$ 0.035) and small

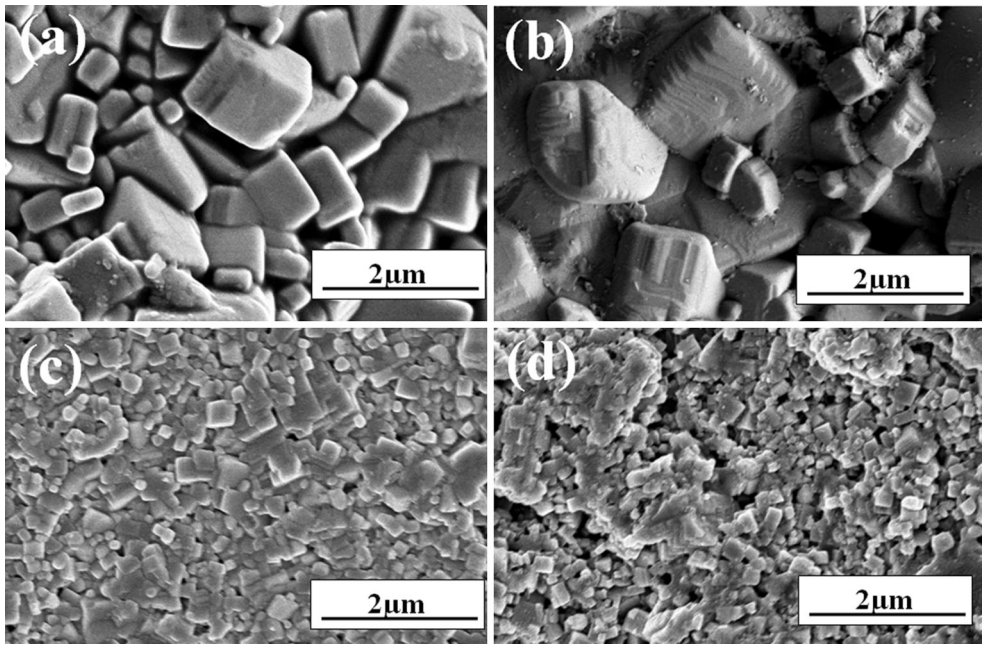

Fig. 2. SEM pictures of the natural surfaces for $(1 - x)$KNN-xBCN with (a) $x = 0.005$, 1145°C, (b) $x = 0.01$, 1145°C, (c) $x = 0.015$, 1155°C, and (d) $x = 0.02$, 1130°C.

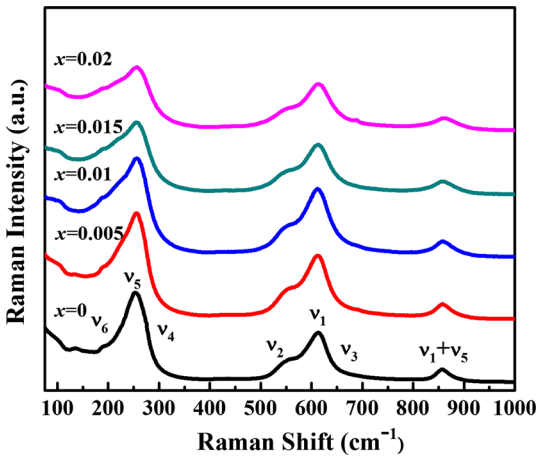

Fig. 3. Room-temperature Raman spectra of $(1 - x)$KNN-xBCN ceramics with $0 \le x \le 0.02$.

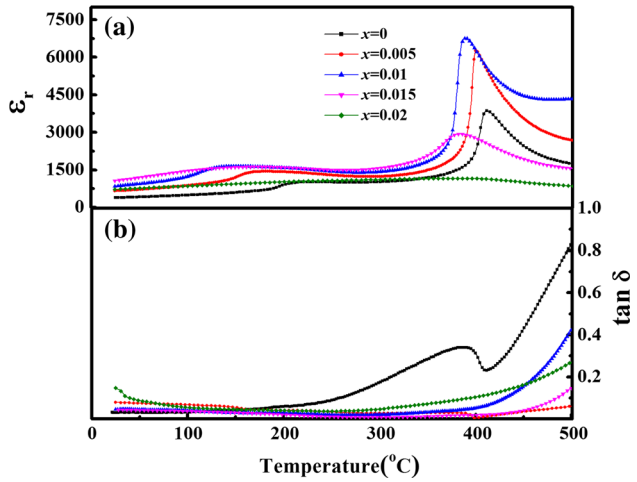

Fig. 4. (a) Temperature dependences of the relative permittivity and (b) dielectric loss for $(1 - x)$KNN-xBCN $(0 \le x \le 0.02)$ ceramics.

$\Delta\varepsilon/\varepsilon_{120°C}$ ($\le \pm 15\%$) over a broad temperature range of 120–342°C. These results indicate that the 0.99KNN–0.01BCN could be applied in high–temperature applications.

Figure 6 illustrates the plots of the $\ln(1/\varepsilon - 1/\varepsilon_m)$ versus $\ln(T - T_m)$ for the $(1 - x)$KNN-xBCN $(0.005 \le x \le 0.015)$ ceramics. γ is the degree of diffuseness which has a value ranging from 1 for a normal ferroelectric to 2 for an ideal relaxor ferroelectric.[28] γ is the slope of the curves, which varies from 1.17 to 1.63, indicating that the $(1 - x)$KNN-xBCN ceramics have transformed from a normal ferroelectric to a relaxor ferroelectric. Figure 7a shows the ferroelectric hysteresis loops (P–E) of $(1 - x)$KNN-xBCN $(0 \le x \le 0.02)$ ceramics measured under a 30-kV/cm electric field at 1HZ. With increasing the BCN content, the remnant polarizations (P_r) firstly increased, reached the maxmium value ($x = 0.01$, 26.52 μm/cm), and then decreased. When $x > 0.01$, the ferroelectric hysteresis loops become flat, indicating a kind of soft ferroelectric behavior of the ceramics. Bipolar electric field-induced strain (S–E) hysteresis loops of $(1 - x)$KNN-xBCN $(0 \le x \le 0.015)$ are presented in

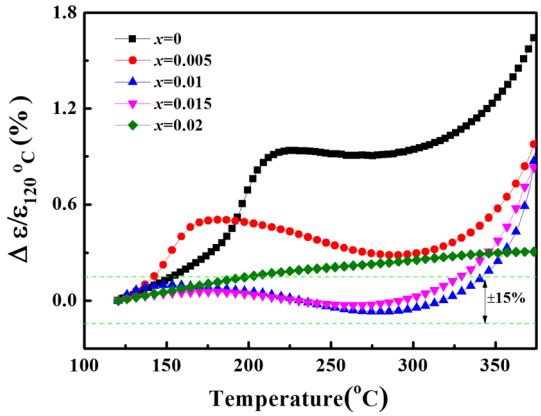

Fig. 5. The temperature coefficient curves of capacitance ($\Delta\varepsilon/\varepsilon_{120°C}$) as a function of the measured temperature from 120°C to 342°C.

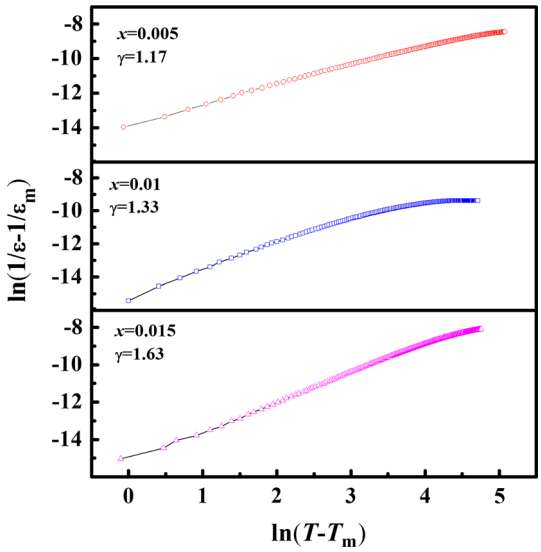

Fig. 6. Plots of $\ln(1/\varepsilon\text{-}1/\varepsilon_m)$ versus $\ln(T - T_m)$ for the $(1 - x)$KNN-xBCN ($0.005 \le x \le 0.015$) ceramics.

Fig. 7b. As $x \le 0.01$, the ceramics exhibited the typical ferroelectric characteristics with a butterfly-shaped strain loop and visible negative strain, S_{neg} ($\sim 0.042\%$), which is similar to that in Dong et al.[29] When $x = 0.015$, the strain hysteresis loops of the samples transformed into a sprout-shaped strain loop with negligible negative strain. These results show that the transition from the ferroelectric to relaxor was induced through changing the composition.

In order to measure the piezoelectric properties of $(1 - x)$KNN-xBCN ceramics, the samples were polarized at 4 kV/mm poling field for 30 min and then cooled to room temperature in the electric field. Figure 8a demonstrates the piezoelectric properties of $(1 - x)$KNN-xBCN ($0 \le x \le 0.02$) as a function of the different poling temperatures. As $x = 0.005$, the optimized piezoelectric properties of the ceramics reached the maximum value, $\sim$ 131 pC/N, at 95°C, which means that there also exists a coexistence of orthorhombic and tetragonal phases in this component. The MBP is the important factor to enhance the piezoelectric properties due to the more polarized directions. As shown in Fig. 8b, the piezoelectric properties of the ceramics decreased with increasing the x values because the PPT temperature, $T_{O\text{-}T}$, shifted to a lower temperature. Figure 8c shows the temperature stability of the piezoelectric for $(1 - x)$KNN-xBCN ($0 \le x \le 0.02$), where the annealing temperature ranges from 50°C to 500°C. When $x \le 0.01$, the ceramics have a good thermal stability of the piezoelectric. Especially, as $x = 0.01$, the sample has a good thermal stability under 350°C ($\sim$ 102 pC/N). When the annealing temperature was above 350°C, the piezoelectric constant rapidly decreased because the temperature is close to T_c, making the center of positive and negative charges of crystal coincide, which could weaken the piezoelectric properties.[30,31]

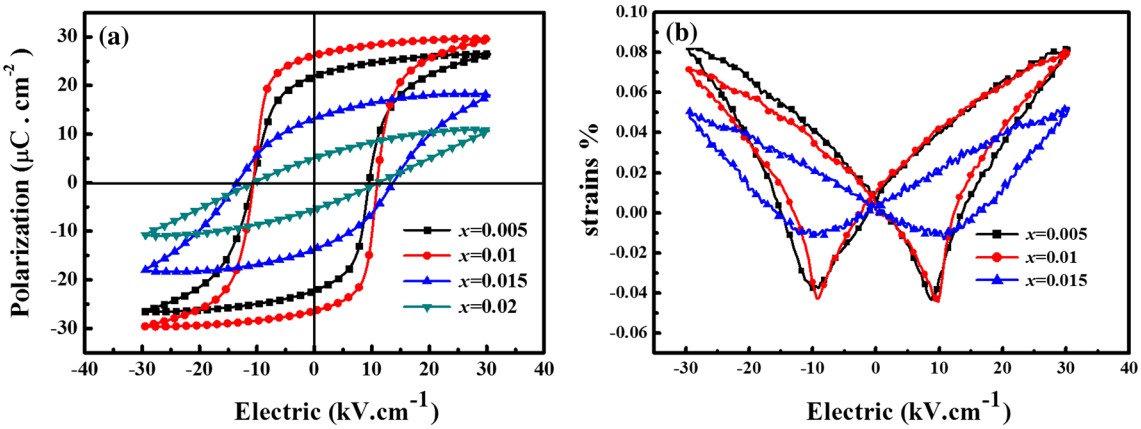

Fig. 7. (a) Ferroelectric hysteresis loops (P–E) of $(1 - x)$KNN-xBCN ($0.005 \le x \le 0.02$) measured at 30 kV/cm at room temperature. (b) The bipolar electric field-induced strain (S–E) hysteresis loops of $(1 - x)$KNN-xBCN ($0.005 \le x \le 0.015$) measured at 30 kV/cm at room temperature.

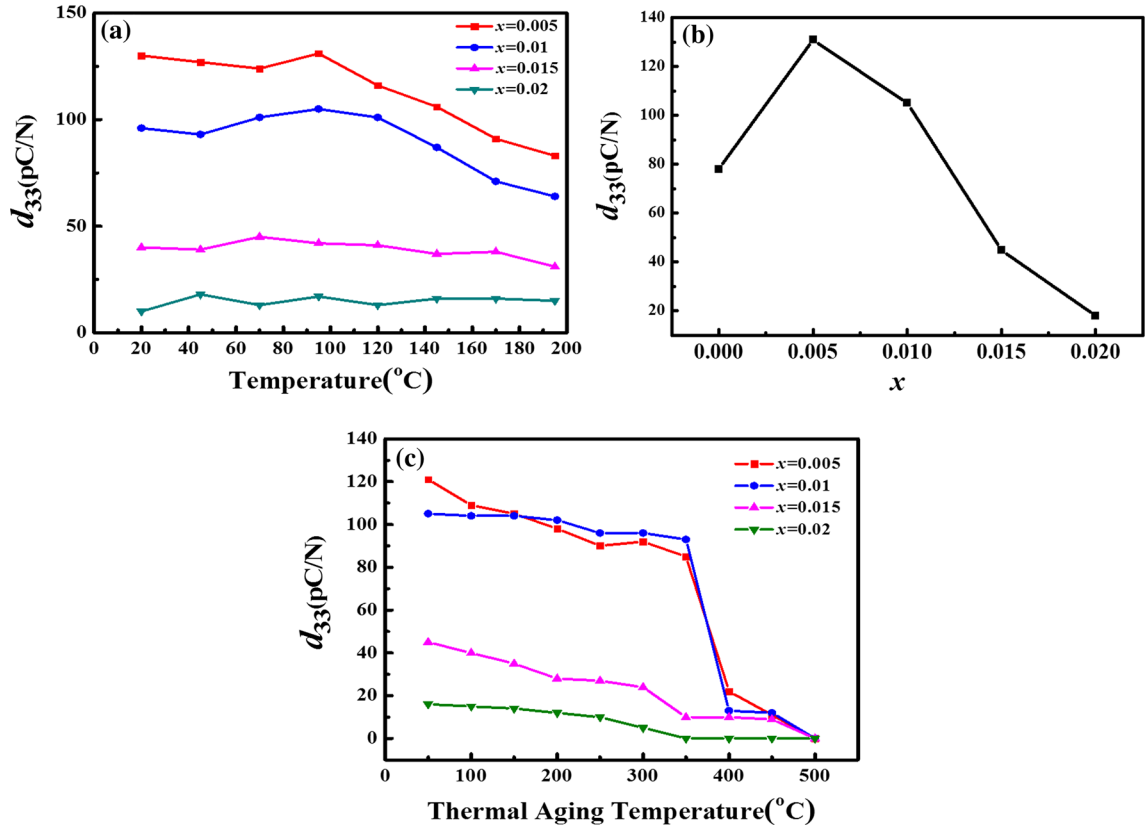

Fig. 8. (a) Piezoelectric properties of (1 − *x*)KNN-*x*BCN (*x* = 0.005, 0.01, 0.015, 0.02) as the function of different poling temperatures. (b) Piezoelectric constant d_{33} of the (1 − *x*)KNN-*x*BCN ceramics as a function of *x* values. (c) Thermal aging temperature dependences of the d_{33} for (1 − *x*)KNN-*x*BCN ($0.005 \le x \le 0.02$) ceramics.

CONCLUSIONS

KNN–BCN lead-free piezoelectric ceramics have been prepared by the traditional solid-state reaction method. A small amount of BCN addition had obvious effects on the microstructure and electrical properties of the KNN ceramics. When $x = 0.01$, the ceramics exhibited small $\Delta\varepsilon/\varepsilon_{120°C}$ ($\le \pm$ 15%) over a broad temperature range from 120°C to 342°C, high relative permittivity ($\sim$ 1502), large remnant polarizations (P_r) of 26.52 μm/cm, visible negative strain $S_{neg} \sim 0.042\%$, large d_{33} of 105 pC/N, good piezoelectric temperature stability and $\tan\delta \le 0.035$. These results indicate that KNN–BCN materials are candidates for high-temperature device applications.

ACKNOWLEDGEMENTS

This work was supported by the Natural Science Foundation of China (Nos. 11664008, 11364012, 11464009 and 61761015), Natural Science Foundation of Guangxi (No. 2015GXNSFDA139033), Research Start-up Funds Doctor of Guilin University of Technology (Nos. 002401003281 and 002401003282) and Project of Outstanding Young Teachers' Training in Higher Education Institutions of Guangxi.

REFERENCES

1. Y. Liu, R.Q. Chu, Z.J. Xu, Y.J. Zhang, Q. Chen, and G.R. Li, *Mater. Sci. Eng. B* 176, 1463 (2011).
2. X.L. Chen, F. He, J. Chen, Y.L. Wang, H.F. Zhou, and L. Fang, *J. Mater. Sci. Mater. Electron.* 25, 2634 (2014).
3. P. Bharathi and B.R. Varma, *J. Electron. Mater.* 43, 493 (2014).
4. H. Ping, P. Henson, and R.W. Johnson, *I.E.E.E. Trans. Ind. Electron.* 58, 2673 (2011).
5. H. Wang, X. Zhai, J.W. Xu, C.L. Yuan, and C.R. Zhou, *J. Electron. Mater.* 24, 2469 (2013).
6. S.J. Zhang, R. Xia, and T.R. Shrout, *J. Electroceram.* 19, 251 (2007).
7. V. Bobnar, M. Hrovat, J. Holc, C. Filipič, A. Levstik, et al., *J. Appl. Phys.* 105, 954 (2009).
8. Y. Guo, K. Kakimoto, and H. Ohsato, *Solid State Commun.* 129, 279 (2004).
9. V. Bobnar, J. Bernard, and M. Kosec, *Appl. Phys. Lett.* 85, 994 (2004).
10. J. Zhao, H. Du, S. Qu, J. Wang, H. Zhang, Y.M. Yang, and Z. Xu, *J. Alloys Compd.* 509, 3537 (2011).
11. E.M. Alkoy and M. Papila, *Ceram. Int.* 36, 1921 (2010).
12. M.H. Zhang, K. Wang, Y.J. Du, G. Dai, W. Sun, G. Li, D. Hu, H.C. Thong, C. Zhao, X.Q. Xi, Z.X. Yue, and J.F. Li, *J. Am. Chem. Soc.* 139, 3889 (2017).

13. F.Z. Yao, K. Wang, W. Jo, K.G. Webber, T.P. Comyn, J.X. Ding, B. Xu, L.Q. Cheng, M.P. Zheng, Y.D. Hou, and J.F. Li, *Adv. Funct. Mater.* 26, 1217 (2016).
14. Y.M. Li, Z.Y. Shen, F. Wu, T.Z. Pan, Z.M. Wang, and Z.G. Xiao, *J. Electron. Mater.* 25, 1028 (2014).
15. K. Kakimoto, K. Akao, Y. Guo, and H. Ohsato, *Jpn. J. Appl. Phys.* 44, 7064 (2005).
16. Y.B. Yao, H.T. Chan, C.L. Mak, and K.H. Wong, *Thin Solid Films* 537, 156 (2013).
17. X.L. Chen, G.F. Liu, G.S. Huang, X.X. Li, X. Yan, and H.F. Zhou, *J. Mater. Sci. Mater. Electron.* 28, 13126 (2017).
18. C.W. Ahn, H.I. Hwang, K.S. Lee, B.M. Jin, S. Park, et al., *J. Appl. Phys.* 49, 095801 (2010).
19. R. Singh, K. Kambale, A.R. Kulkarni, and C.S. Harendranath, *Mater. Chem. Phys.* 138, 905 (2013).
20. R. Wang, R.J. Xie, K. Hanada, K. Matsusaki, H. Bando, and M. Itoh, *Phys. Status Solidi Appl. Mater.* 202, R57 (2005).
21. T. Zheng, H.J. Wu, Y. Yuan, X. Lv, Q. Li, T.L. Men, C.L. Zhao, D.Q. Xiao, J.G. Wu, K. Wang, J.F. Li, Y.L. Gu, J.G. Zhua, and S.J. Pennycook, *Energy Environ. Sci.* 10, 528 (2017).
22. W.L. Zhu, J.L. Zhu, Y. Meng, M.S. Wang, B. Zhu, et al., *J. Phys. D Appl. Phys.* 44, 505303 (2011).
23. X.P. Wang, J.G. Wu, D.Q. Xiao, J.G. Zhu, X.J. Cheng, T. Zheng, B.Y. Zhang, X.J. Lou, and X.J. Wang, *J. Am. Chem. Soc.* 136, 2905 (2014).
24. K. Xu, J. Li, X. Lv, J.G. Wu, X.X. Zhang, D.Q. Xiao, and J.G. Zhu, *Adv. Mater.* 28, 8519 (2016).
25. M. Sutapun, C.C. Huang, D.P. Cann, and N. Vittayakorn, *J. Alloys Compd.* 479, 462 (2009).
26. H.L. Du, W.C. Zhou, F. Luo, D.M. Zhu, S.B. Qu, Y. Li, and Z.B. Pei, *J. Appl. Phys.* 104, 034104 (2008).
27. H.L. Du, W.C. Zhou, F. Luo, D.M. Zhu, S.B. Qu, Y. Li, and Z.B. Pei, *J. Phys. D Appl. Phys.* 41, 085416 (2008).
28. D. Lin, K.W. Kwok, and H.L.W. Chan, *J. Phys. D Appl. Phys.* 40, 6778 (2007).
29. G.Z. Dong, H.Q. Fan, J. Shi, and M. Li, *J. Am. Ceram. Soc.* 98, 1150 (2014).
30. J.G. Wu, D.Q. Xiao, and J.G. Zhu, *Chem. Rev.* 115, 2559 (2015).
31. H.L. Du, W.C. Zhou, F. Luo, D.M. Zhu, S.B. Qu, and Z.B. Pei, *Appl. Phys. Lett.* 91, 202907 (2007).